Could bulk density profiles provide information about recent sedimentation rates?

José-María Abril

Abstract

Independent validation has to be an integral part of the ^{210}Pb-based radiometric dating of recent sediments. The combined use of artificial fallout radionuclides leads to serious problems because only the identification of peaks and their use as time-marks is not sufficiently rigorous to ensure the accuracy of dates. Quantitative modelling of depth profiles requires reliable input functions, which can be substantially different from the atmo-spheric deposition records. The appropriate treatment of compaction is another source of complexity. Continuum mechanics provide a suitable framework to understand compaction in sedimentary basins with length scales of several km. Nevertheless, early compaction (with length scales of few cm at the sediment surface) takes place under hydrostatic equilibrium conditions, and it can be better understood as a transport phenomenon: a mass flow governed by spatial gradients of a compaction-potential energy, involving a conductivity function. This paper explores some analytical and numerical solutions for these equations to provide insight about the early compaction phenomenon. Given a conductivity function and a constant sedimentation rate, the system will evolve towards a steady-state profile for bulk density. The fingerprint of variable sedimentation rates, among other changes in environmental conditions, will be studied with numerical solutions. Finally, the paper explores the use of bulk density profiles for deriving information on recent sedimentation rates, which could provide independent support for the radiometric dating models.

Keywords Bulk density · Early compaction · Sedimentation rate · Radiometric dating · Mass depth

Abbreviations
SWI   Sediment–water interface
ECL   Early compaction limit

J.-M. Abril (✉)
Dpto. Física Aplicada I, Universidad de Sevilla, ETSIA, Ctra Utrera Km 1, 41013 Seville, Spain
e-mail: jmabril@us.es

Introduction

Radiometric dating of recent sediments can provide sedimentation rates and dates. Chronologies from ^{210}Pb have been used widely for this purpose, with application of different radiometric dating models. A radiometric dating model has to be understood as a particular solution based on the general and unique physical problem of mass conservation of solids, and for the particle-associated tracers, in sediments that undergo accretion and compaction (Abril 2003a).

The most important limitation arises when a chronology cannot be unambiguously established (Robbins 1978; Smith 2001). The question is usually solved by the combined use of ^{210}Pb and artificial fallout radionuclides. Nevertheless, the identification of peaks and their use as time-marks is not confident enough (Abril 2003b, 2004). The quantitative modeling of their depth profiles requires reliable input functions as boundary conditions, but radioactive fluxes onto the sediment can be substantially different from the known atmospheric deposition records (Abril et al. 1992; Abril and García-León 1994; Robbins et al. 2000; Appleby 2001; Laissaoui et al. 2008). In addition, early compaction will complicate the specific activity profiles. In this context, it is interesting to examine the potential use of bulk density profiles to assist the radiometric dating of recent sediments.

In sedimentary basin research, continuum mechanics is used to model gravitational compaction. The first basic premise is that the rate of gravitational compaction is limited by low permeability of the sediments, which are treated as a two-phase continuum. Thus, interstitial fluids would help to support the increasing overburden weight (Chilingarian et al. 1995). Such models typically involve length scales of several km, usually apply to steady-state compaction, and they do not account for the ubiquitous and steep porosity gradients near the sediment-water interface (SWI).

Some attempts have been made to apply the same approach to model bulk density profiles near the SWI. Fukumori et al. (1992) used a formulation involving the Young's module, which is written as an analytical function of bulk density as established ad hoc, after the fit of the measured bulk density profile to a potential function. Meysman et al. (2005) used the saturated soil stress balance to develop a formally closed system of differential equations, but in the applications, they used, as a practical approach, the empirical bulk density profiles instead of solving the governing equations. Jourabchi et al. (2010) applied a similar approach, but using constitutive equations for hydraulic conductivity and a compressive response coefficient, and they used inverse numerical modelling to estimate the mass sedimentation rates. This method was limited to steady-state situations, and it showed high sensitivity because of the compressive response coefficient.

The SWI region usually has high porosity and it is relatively more permeable. As long as the fluid can escape under normal loading conditions and porosity is intercommunicating, hydrostatic pressures will be encountered (Chilingarian et al. 1995). Under these conditions, the early compaction could be better understood as a phenomenon of reallocation of solid particles under the action of the stirring and the gravitational field (Abril 2003a). In this treatment of the early compaction, the associated mass flow was described by a linear transport equation, involving the spatial gradients of a compaction potential energy, and a conductivity function.

This paper tries to examine more deeply the formulation of the compaction potential energy and the conductivity function. Typical bulk density profiles show an asymptotic increase with depth, with the scaling factor being governed by the conductivity function and the sedimentation rate. The governing equation will be numerically solved for a wide variety of scenarios to explore the distinctive chronological marks in bulk density profiles from varying sedimentation environments.

Materials and methods

Theory development

The continuity equation for solids in a sediment core

As result of the accumulation of new material over a sediment core, its SWI displaces upwards. From a framework anchored to this boundary, the whole sediment moves down with the sedimentation velocity v [L T^{-1}] (v can be a function of time but not of depth, z [L], measured downwards).

Bulk density, ρ [M L^{-3}], is the mass of dry matter per unit volume of undisturbed sediment. Local horizontal homogeneity will be assumed, in such a way that only changes with depth are relevant (a one-dimensional problem). Symmetric exchanges (with null averaged mass flow) of solid (or water) volumes through any arbitrary horizon will not contribute to changes in bulk density, but they contribute, as diffusion, to changes in the bulk concentrations of particle-associated tracers. The replacement of pore-water by a solid particle affects bulk densities. This

process is forced by the gravity field, and can be described as a mass flow (Abril 2003a):

$$\rho q = -K\frac{\partial \psi}{\partial z} \tag{1}$$

Equation 1 is similar to the linear transport equations of classical physics, being q [L T^{-1}] the velocity associated with the flow of solids, ψ [L] the specific potential energy for solid particles or the compaction potential, and K [M L^{-2} T^{-1}] is a conductivity function (Table 1 summarises the symbols used in this paper). Conceptually, the spatial gradients of ψ can only be upwardly directed. We can imagine this mass flow as the result of a relatively uniform reduction of the size of pore spaces, preserving the main structure of a sediment layer (a "varve" if we want), but it can equally involve the reallocation of solids, with the colloidal and the small-grain-size fractions "moving" through the connected porewaters.

The continuity equation can be then written as follows (Abril 2003a):

$$\frac{\partial \rho}{\partial t} = -\frac{\partial}{\partial z}(\rho v + \rho q) \tag{2}$$

Let us introduce the magnitude $w = \rho v + \rho q$ [M L^{-2} T^{-1}] as the mass flow of solids at any sediment horizon at depth z and time t. At the SWI, $w(0,t)$ is just the mass input, or the mass sedimentation rate, w_0. At depths large enough (mathematically $z \to \infty$, but in practice some tens of cm) the mass flow due to early compaction vanishes ($\rho q \to 0$), and then $w(\infty, t) = \rho_\infty v(t)$. It is worth noting that the present formulation of the theory explicitly is limited to the effects of early compaction, the ubiquitous and steep gradients of porosity near the SWI. It is also limited to situations where the physical processes (the forced mass flow) are dominant. Other limnological, geochemical and biogeochemical processes can affect or even govern such a mass flow under some particular situations, which falls beyond the scope of the present work.

For steady-state bulk density profiles $\left(\frac{\partial \rho}{\partial t} = 0\right)$, Eq. 2 requires $\frac{\partial w}{\partial z} = 0$. That is, the flow of matter through the sediment has to be continuous (there is not accumulation nor sources of material within the sediment), and w can be a function of time but not of depth. In this situation $w_0 = v\rho_\infty$; and then,

$$\rho q = w_0\left(1 - \frac{\rho}{\rho_\infty}\right). \tag{3}$$

Figure 1 shows ρq and q for a typical asymptotic bulk density profile given by

$$\rho = \rho_\infty - \rho_1 e^{-\alpha z}, \tag{4}$$

where α [L^{-1}] is an scaling factor, and ρ_1 the bulk density gap between $z = 0$, and $z \to \infty : \rho_1 = \rho_\infty - \rho_0$.

It can be demonstrated (Abril 2003a) that Eq. 4 arises as the particular steady-state solution for Eq. 2 under constant K and v, when the compaction potential is a linear function of ρ. Alternatively, Eq. 4 arises as the steady-state solution under constant spatial gradients of ψ and depth-dependent conductivities, and as shown later, it seems to be a more appropriate description of early compaction.

The compaction potential

Let be ρ_s and ρ_w the density of solids and pore water, respectively. Being $\rho_s > \rho_w$, in a gravity field, a solid particle tends to occupy the space of porewater under it, unless the contact forces from other solid particles prevent it. In this process the specific potential energy of the system decreases. Thus, in the situation depicted in Fig. 2, the joint initial gravitational-potential energy of a differential volume dV occupied by a solid particle, at depth z, and porewater of the same volume at depth $z + dz$, will be (referred to a datum at depth z_D):

$$E_{p,i} = \rho_s g dV(z_D - z) + \rho_w g dV(z_D - z - dz)$$

When the solid particle replaces the porewater, the new potential energy is

$$E_{p,f} = \rho_s g dV(z_D - z - dz) + \rho_w g dV(z_D - z)$$

The variation in this potential energy divided by the weight of the solid particle, $\rho_s g dV$, is the change in the compaction potential dψ:

$$d\psi = -\frac{\rho_s - \rho_w}{\rho_s}dz$$

or, by grouping the densities in the factor β (the buoyancy):

$$\frac{\partial \psi}{\partial z} = -\beta \tag{5}$$

Table 1 List of symbols used (M = Mass, L = length, T = time)

ρ_s, ρ_w	M L^{-3}	Density of solids and water in a sediment core
z	L	Actual depth, measured downwards from the SWI
z_D	L	Depth of a reference Datum
t	T	Time
ρ	M L^{-3}	Bulk density
ρ_0	M L^{-3}	Value of ρ at SWI
ρ_∞	M L^{-3}	Value of ρ at depths greater than the early compaction limit (ECL)
$\rho_1 = \rho_\infty - \rho_0$	M L^{-3}	Bulk density lag at SWI
$\rho_D(z) = \rho_\infty - \rho(z)$	M L^{-3}	Default bulk density
$dm = \rho dz$	M L^{-2}	Differential mass thickness
$m = \int_0^z dm$	M L^{-2}	Mass depth
$\phi = (1 - \rho/\rho_s)$	–	Porosity, ratio between volume of pore water and the bulk volume
ϕ_0, ϕ_∞	–	Porosity at SWI, porosity at depths > ECL
$\phi_1 = \phi_0 - \phi_\infty$	–	Porosity excess at SWI
$\phi_{exc} = \phi_0 - \phi(z)$	–	Excess porosity at depth z
α	L^{-1}	Scaling factor for $\rho(z) = \rho_\infty - \rho_1 e^{-\alpha z}$
α_m	M^{-1} L^2	Scaling factor for $\rho(m) = \rho_\infty - \rho_1 e^{-\alpha_m m}$
v	L T^{-1}	Sedimentation velocity (the SWI displaces up with this velocity)
q	L T^{-1}	Velocity associated to the mass flow of solids due to compaction
$w(z,t) = \rho(v + q)$	M L^{-2} T^{-1}	Mass flow of solids at any sediment horizon at depth z and time t
$w_0 = w(0,t)$	M L^{-2} T^{-1}	Sedimentation rate: mass flow of solids at the SWI
ψ	L	Compaction potential: specific potential energy for solid particles
K	M L^{-2} T^{-1}	Conductivity for the mass flow of solids
K_0	M L^{-2} T^{-1}	Conductivity at the SWI
g	L T^{-2}	Gravitational acceleration
$E_p, E_{p,i}, E_{p,f}$	M L^2 T^{-2}	Gravitational potential energy; initial and final values.
dV	L^3	Differential volume element
$\beta = (\rho_s - \rho_w)/\rho_s$	–	Buoyancy
σ	M L^{-1} T^{-2}	Effective stress supported by the solid skeleton of the sediment
δW	M L^2 T^{-2}	Virtual work associated to a virtual displacement δz
A	M L^{-2} T^{-1}	Constant of proportionality (site specific) for $K = A\phi_{exc}$
C_z	T^{-1}	Constant of proportionality (site specific) for $\frac{\partial K}{\partial z} = -C_z\rho_D$
C_m	M^{-1}L^3 T^{-1}	Constant of proportionality (site specific) for $\frac{\partial K}{\partial m} = -C_m\rho_D$
ρ'	M L^{-3}	Fluctuations of ρ around its time-averaged value
v'	L T^{-1}	Fluctuations of v around its time-averaged value
σ_t	T	Time parameter in a Gaussian pulse
Δt	T	Time step used in the finite-differences numerical scheme
Δz	L	Depth step used in the finite-differences numerical scheme

Thus, the spatial gradient of compaction potential is upwardly directed and has an approximately constant value (unless changes in mineralogical composition and organic matter content). For typical values of 2.5 and 1.0 g cm^{-3} for ρ_s and ρ_w, respectively, $\beta = 0.6$ (dimensionless). Equation 5 can be integrated to obtain $\psi(z)$, after fixing any arbitrary reference point (e.g. $\psi(0) = 0$).

The same result can be found using the concept of overburden potential under hydrostatic equilibrium (Chilingarian et al. 1995). The spatial derivative of the effective stress supported by the solid skeleton, σ,
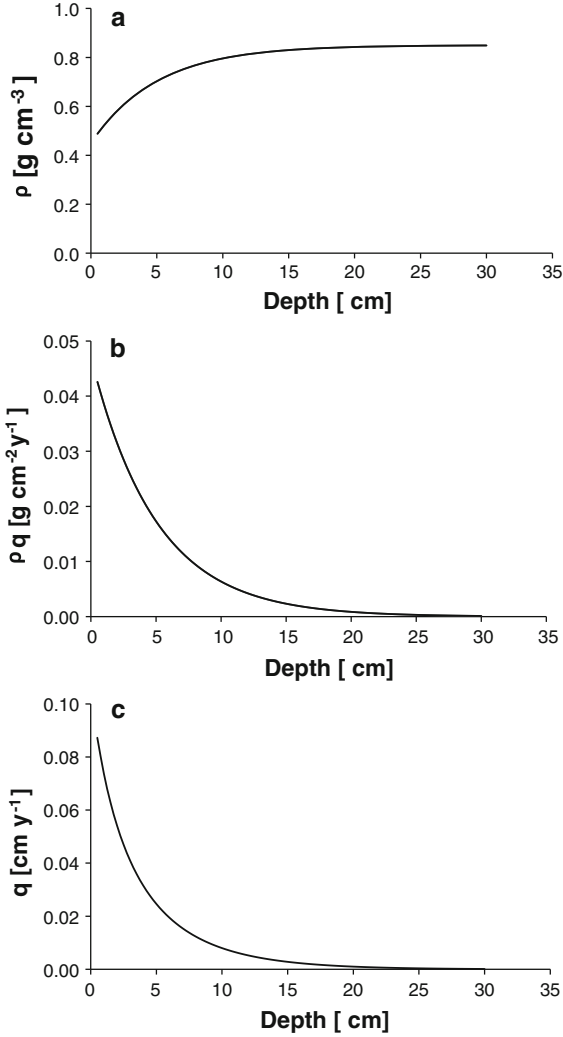
Fig. 1 Bulk density profile given by Eq. 4 with $\rho_\infty = 0.85$ g cm^{-3}, $\rho_1 = 0.4$ g cm^{-3}, $\alpha = 0.2$ cm^{-1} and $w = 0.1$ g cm^{-2} year^{-1}, the steady state mass flow, ρq, associated with early compaction (from Eq. 3), and the velocity q versus depth in the sediment core

is: $\frac{\partial \sigma}{\partial z} = -\beta g \rho$. As this stress is null at the SWI, $\sigma = \beta g m$, where m is the mass depth $\left(m = \int_0^z \rho \, dz'\right)$. Let us imagine a sediment column of mass depth m and unit cross-sectional area, which is able to compress the sediment below it acting against the effective stress. The virtual work associated with a virtual displacement, $\delta W = \sigma dz$, results in a decrease of its potential energy, and in terms of potential energy per unit weight:
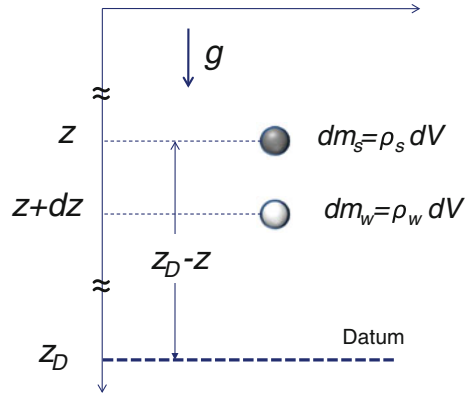

Fig. 2 Scheme illustrating the change in gravitational potential energy associated with the elemental process of exchange of a solid particle by interstitial water lying below it

$$\frac{\delta W}{mg} = \frac{\sigma \delta z}{mg} = \beta \delta z = -\delta \psi$$

Conductivity

Let us consider the steady-state situation of Eq. 3, combined with Eqs. 1 and 5 to solve the conductivity:

$$K = \frac{w_0}{\beta}\left(1 - \frac{\rho}{\rho_\infty}\right),$$
$$K = \frac{w_0}{\beta}\frac{\rho_1}{\rho_\infty}e^{-\alpha z}. \tag{6}$$

The last expression applies to steady-state bulk densities given by Eq. 4. The exponential decrease of conductivity with depth can be understood in terms of a progressive reduction in porewater space. Porosity, ϕ, the ratio between the volume occupied by porewater and the bulk volume, is related to the bulk density:

$$\rho = \rho_s(1 - \phi)$$

For bulk density profiles given by Eq. 4, $\phi(z) = \phi_\infty + \phi_1 e^{-\alpha z}$, with $\phi_1 = \frac{\rho_1}{\rho_s}$ being the "excess" porosity at the SWI with respect to the porosity at great depths, where early compaction does not have further effect. Thus,

$$K(z) = \frac{w_0}{\beta}\frac{\rho_s}{\rho_\infty}\phi_1 e^{-\alpha z} = A\phi_1 e^{-\alpha z}, \tag{7}$$

where the constants have been grouped in the factor A. This is, under constant sedimentation rate and steady-state bulk density profiles given by Eq. 4, the

conductivity is proportional to the "excess" porosity $\phi_{\text{exc}} = \phi - \phi_\infty$.

To properly interpret Eq. 7, it is important to note that if bulk density is steady state and given by Eq. 4, then conductivity is necessarily given by Eq. 7. This is not a sufficient condition to generate steady-state bulk density profiles as those of Eq. 4, only from the continuity equation (Eq. 2). For this purpose, it is necessary to explicitly note that conductivity decreases with depth, its rate of change being proportional to the "missing" or the default bulk density, ρ_D, defined as $\rho_D = \rho_\infty - \rho$ (or $\rho_D = \rho_s \phi_{\text{exc}}$):

$$\frac{\partial K}{\partial z} = -C_z \rho_D. \tag{8}$$

This law is justified from a mathematical point of view because it is able to produce suitable steady-state solutions. Its physical meaning is that as the capability of sediment for "transporting" solids increases, the chance of reduction of pore spaces downstream will be greater, thus decreasing conductivity.

Let us take spatial derivatives in Eq. 6 (applicable for steady-state bulk densities) using Eq. 8 and the definition of ρ_D:

$$-C_z \rho_D = \frac{w_0}{\beta \rho_\infty} \frac{\partial \rho_D}{\partial z}.$$

By grouping terms and integrating from the SWI down to a depth z,

$$\rho_D = \rho_1 e^{-\alpha z},$$

with ρ_1 as defined in Eq. 4, and $\alpha = \frac{\beta C_z \rho_\infty}{w_0}$, the scaling factor. This solution corresponds with the one of Eq. 4. Solving now for $K(z)$ from Eq. 8:

$$K(z) = \frac{C_z}{\alpha} \rho_1 e^{-\alpha z} + D$$

But $D = 0$, because conductivity must vanish for great depths. This solution corresponds with the right-hand side of Eq. 7, being $C_z = A\alpha/\rho_s$.

The scaling factor defining the steady-state distribution of bulk densities is governed by the supply of matter onto the sediment and the rate of change in its ability for transporting this material through pore spaces. This is the first point of interest in terms of sediment dating: if the conductivity function could be independently established (and the inter-comparison

of physical properties in a wide set of sediment cores can be a way to confine it), then sedimentation rate could be solved from the parameters defining the bulk density profile, when this follows Eq. 4.

To better understand how the conductivity function works, let us consider the following sequence of ideal situations.

(a) There is not a matter supplied to the sediment and the contact forces are able to support the sediment structure, resulting in a null value for conductivity (also in this situation $v = 0$). Then, following Eq. 2, the bulk density necessarily will be steady state $\left(\frac{\partial \rho}{\partial t} = 0\right)$.

(b) There is not supply of matter, but conductivity is not null (e.g., pressure waves, micro-earthquakes, and other sources of stirring promote the reallocation of solids within the sediment core). As at the SWI there is no flow of matter:

$$0 = v\rho_0 + \beta K_0,$$

where ρ_0 and K_0 are, respectively, the bulk density and the value of conductivity at the interface. Consequently, the velocity takes negative values (the SWI collapses, which is seen from the framework that is related to it as a net upward displacement of the sediment core):

$$v = -\frac{\beta}{\rho_0} K_0.$$

If initial conditions for ρ were given by Eq. 4, then the initial rate of change in bulk density can be obtained from Eq. 2 (using Eqs. 1, 5):

$$\frac{\partial \rho(z, t)}{\partial t} = \frac{\alpha \beta K_0 \rho_1}{\rho_0} e^{-\alpha z} - \beta \frac{\partial K}{\partial z}.$$

If one can assume K being proportional to the excess porosity (as in Eq. 8), then the initial rate of change in bulk density is positive, and it will decrease exponentially with depth with the same scaling factor α.

(c) There is a matter supply onto the sediment, w_0, while the conductivity has a null value.

The boundary condition at the SWI provides $v = w_0/\rho_0^*$; and the initial rate of change in bulk densities (assuming initial conditions by Eq. 4) is

$$\frac{\partial \rho(z,t)}{\partial t} = -\frac{\alpha w_0 \rho_1}{\rho_0^*} \, \mathrm{e}^{-\alpha z}$$

While the undisturbed profile displaces downwards, low density values are now seen deeper in the core, with the rate of change decreasing with depth. We note that in this equation ρ_0^* can be different from the initial value of bulk density at the interface.

The previous examples have to be completed within the context of an input of matter combined with a non-null conductivity. This set of different situations helps us to imagine a real situation in which the states of equilibrium are alternating with episodic perturbations on both inputs of matter and conductivities. Thus, the governing differential equations have to be understood in terms of time (and cross-sectionally) averaged variables, over time intervals large enough to include a representative sequence of all these situations, but small enough in relation to the involved time scales so that differential laws still preserve their physical meaning.

More rigorously, when the involved magnitudes ρ, v and K are written as the sum of their averaged values plus a fluctuation, the time-averaging of Eq. 2 preserves its form, involving now only the time-averaged magnitudes, but a new term arises, involving the product of the fluctuations in density and velocity (time average is indicated with the symbol $\langle \rangle$ and $'$ denotes the fluctuation):

$$-\frac{\partial}{\partial z}\langle \rho' v' \rangle.$$

A similar situation appears in the treatment of the Reynold's equations for a turbulent fluid, but involving the product of the fluctuations in two components of the velocity, which contribute to the diffusive transport. In fact, this depends on how these two magnitudes are correlated. In the above discussed situation (b), the velocity will be lower than the average over a variety of different situations, and thus $v' < 0$, while the initial rate of change in ρ is positive, what can be interpreted as $\rho' > 0$. Similarly, in the situation (c) $v' > 0$ and $\rho' < 0$. In both cases the contribution to $\langle \rho' v' \rangle$ has the same sign. Thus, one can expect a net contribution of this term, but at this stage there is not enough support to formally introduce a diffusion term in Eq. 2 In what follows, and in order to get a basic understanding of the theory of early compaction, this term will be neglected in the continuity equation.

The numerical problem

For non-steady-state situations, the set of Eqs. 2 and 8 can be numerically solved, with the following boundary conditions:

- $\rho(\infty, t) = \rho_\infty$. There is an early compaction limit (ECL) which depends on the properties of solid particles. This magnitude is an observable in the sediment core. Here, the infinite has to be understood as a depth large enough as to reach the ECL.
- $\rho(0, t) = \rho_0(t)$. The bulk density at the SWI depends on the properties of the settling material. Here $\rho_0(t) = \rho_0$ will be assumed, being this magnitude an observable in the sediment core.
- $K(\infty, t) = 0$. Conductivity vanishes at the ECL.
- $w_0(t) = v(t)\rho_0 + \beta K(0,t)$. Sedimentation rates will be provided as boundary conditions, and this equation will serve to solve $v(t)$.

Initial conditions are required. Here Eq. 4 will provide $\rho(z,0)$.

The values of C_z (Eq. 8) and β have to be specified.

The numerical solution requires the spatial and temporal discretization of the equations, involving increments of Δz and Δt, respectively. Bulk densities will be evaluated at $z + \Delta z/2$, and the mass flows at $z + \Delta z$. A finite difference scheme will be applied, centred in the space for $v\rho$, and forwarded in time. At each time interval, $K(z,t)$ will be obtained by integration from bottom to top:

$$K(z,t) = \int\limits_{\infty}^{z} -C_z \rho(z',t)\mathrm{d}z'.$$

The value of $K(0,t)$ allows us to estimate $v(t)$ from the last boundary condition, and then allow us to use it to solve Eq. 2 for ρ.

It is important to note that if the value of C_z could be independently stated, then an inverse modelling technique could provide the value of the sedimentation rate.

Results

Steady state profiles under constant C_z and w

The following parameter values and discretization details have been used in these numerical exercises

(hereafter units are cm for L, year for T, and gram for M—see dimensions in Table 1):

- Initial conditions: $\rho_\infty = 0.85$; $\rho_1 = 0.50$; $\alpha = 0.20$
- Spatial gradient of compaction potential: $\beta = 0.6$.
- Discretization: $\Delta z = 0.1$; $\Delta t = 0.005$; total depth 30 cm, and time of simulation 150 year (to ensure convergence towards the steady-state solutions).

The first simulation is devoted to demonstrate self consistence of equations and the accuracy of the numerical method, using a constant $w_0 = 0.10$, and $C_z = 0.0392$, this last coming from the steady state solution:

$$C_z = w_0 \alpha / (\beta \rho_\infty). \qquad (9)$$

The solution is shown in Fig. 3 (curve "R1"), which matches the analytical solution.

Starting from the same initial conditions a double value for C_z is imposed, keeping the sedimentation rate constant ($w_0 = 0.10$). The system evolves towards a new steady-state situation, in which the scaling factor takes a double value (from Eq. 9). The numerical solution (R2) is shown in Fig. 3, along with the corresponding analytical solution.
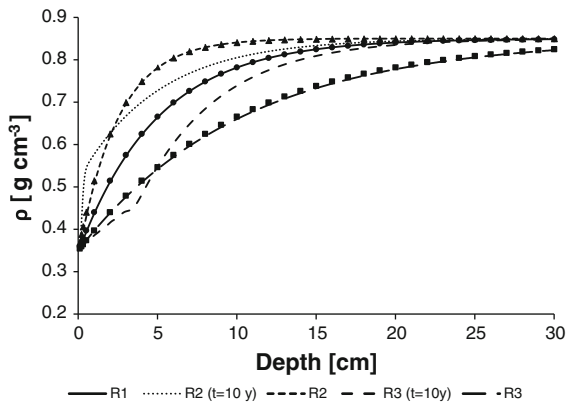

Fig. 3 Bulk density profiles generated as numerical solutions of Eqs. 2 and 8. Initial conditions are, in all the cases, $\rho_\infty = 0.85$ g cm^{-3}, $\rho_1 = 0.5$ g cm^{-3} and $\alpha = 0.2$ cm^{-1}. Curve R1 uses $w_0 = 0.1$ g cm^{-2} year^{-1} and C = 0.0392 year^{-1} (from Eq. 9) and $t = 150$ year; R2 is as R1 but with double C value, and R3 as R1 but with double w_0. Curves are compared with corresponding analytical solutions (*circles*, *triangles* and *squares*, respectively). R2[$t = 10$ year] and R3[$t = 10$ year] illustrate the transient regimen for a time $t = 10$ year after imposing forcing conditions

Using again the initial conditions from R1, the value of C_z is maintained, but sedimentation rate is doubled. A new steady sate is generated, with the scaling factor taking its half value (as expected from Eq. 9). The solution (R3) is shown in Fig. 3, and compared against the analytical solution.

Curves R2[$t = 10$ year] and R3[$t = 10$ year] illustrate the transient regimen, for a time $t = 10$ year after imposing the respective forcing conditions.

Time-dependent sedimentation rates
and boundary conditions

This section explores the effects of varying sedimentation conditions on bulk density profiles. The first simulation uses the same initial conditions and value of C_z than for R1, while sedimentation rate follows a periodic function, with a period of 7 years:

$$w_0(t) = 0.10 + 0.05 \cos\left(\frac{2\pi}{7} t\right)$$

Here, the amplitude of changes in w_0 is small enough to maintain positive sedimentation velocities. Thus, the resulting bulk density profile (after a simulated time of 150 year) shows small fluctuation around the corresponding analytical solution for the steady-state case with the averaged value of sedimentation rate (Fig. 4, R4). Curve R4b in Fig. 4 is as R4 but with amplitude 0.08 g cm^{-2} year^{-1}.

Curves R5 and R6 in Fig. 4 correspond, respectively, to two episodic events of increasing/decreasing sedimentation rates, simulated as a Gaussian pulse taking place at time $t = 140$ year (this is 10 years before the final state shown in the simulation) with a $\sigma_t = 1$ year and a net input of 0.20 g cm^{-2}.

The curve R7 in Fig. 4 simulates a uniform acceleration in recent sedimentation rates, and it uses the same initial conditions and C_z value than R1, and $w_0 = 0.10$ for $t < 130$ year, while for $t \geq 130$, a constant acceleration of 0.007 g cm^{-2} year^{-2} was imposed.

Finally, R8 in Fig. 4 is as R1 but with periodic changes in ρ_0 during the last 50 years (amplitude 0.1 g cm^{-3} and period 7 year).

Estimation of recent sedimentation rates
from typical steady-state bulk density profiles

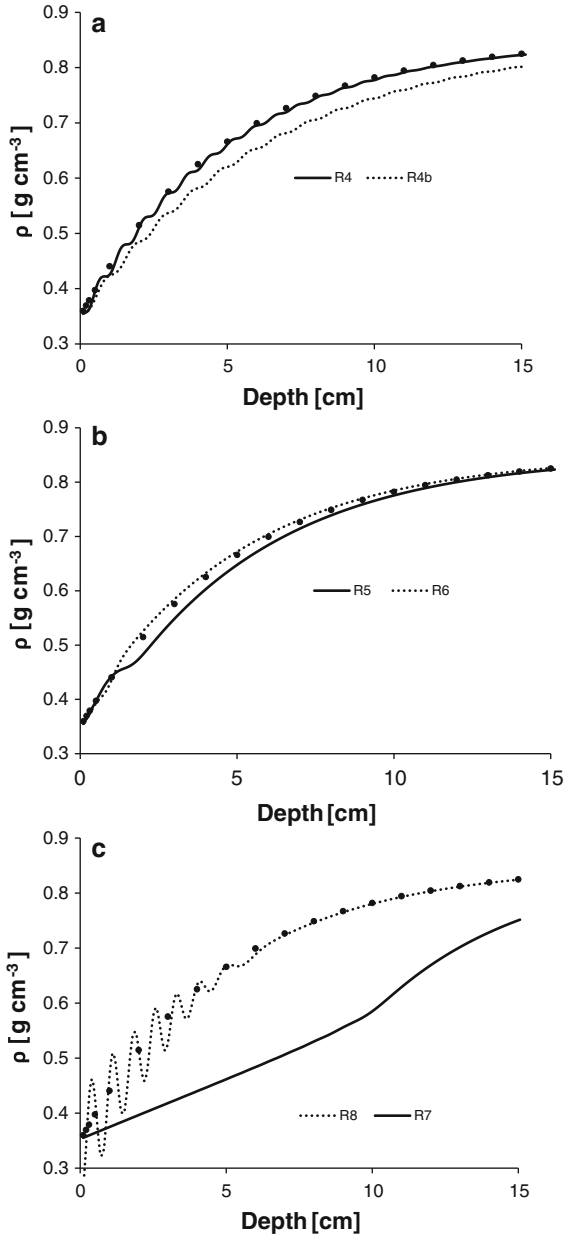This approach is limited to sediment cores for which ρ reasonably fits Eq. 4, and can be assumed as

Fig. 4 As in Fig. 3. Curve R4 uses the same parameters as in R1 but with periodic changes in w_0 (average and amplitude 0.1 and 0.05 g cm^{-2} year^{-1}, respectively, period 7 year). Curve R4b is as R4 but with amplitude of 0.08 g cm^{-2} year^{-1}. Curves R5 and R6 simulate a Gaussian episodic event of increase/decrease in w_0, with $\sigma_t = 1$ year. Curve R7 is as R1, but with a constant acceleration of 0.007 g cm^{-2} year^{-1} in w_0 during the last 30 year. Curve R8 is as R1 but with periodic changes in ρ_0 during the last 50 years (amplitude 0.1 g cm^{-3} and period 7 year). The corresponding analytical solution for R1 is depicted (*circles*) for the sake of comparison

steady-state. Consequently, w has to be uniform or it co-varies with conductivity, as deduced from Eq. 6. As seen in the previous section, some transient situations can be also indistinguishable in practice from the steady state.

Let us assume that in Eq. 7 the value of A can be independently stated. Then the sedimentation rate will be

$$w_0 = A\beta \frac{\rho_\infty}{\rho_s}. \tag{10}$$

For each particular sediment core, A is assumed to be constant, but when comparing different cores, it is expected that some dependence will occur with sediment parameters and hydraulic pressure. The bulk density at the compaction limit, ρ_∞, and ρ_0, can include information on granulometry and mineralogical characteristics. Conductivity will depend on a variety of factors, such as the ability of solid particles to arrange different packing orders or to move through the connected pore spaces.

Table 2, in the Electronic Supplementary Material (ESM), compiles values for ρ_∞, ρ_1, α, water depth and w_0 for a selected set of cores, taken from literature data (Robbins and Edgington 1975; Christensen and Bhunia 1986; Wan et al. 1987; Buffoni et al. 1992; Crusius and Anderson 1995a, b; Muñoz et al. 2004; Erlinger et al. 2008; Laissaoui et al. 2008; Jourabchi et al. 2010). Equation 10 has been used to estimate the value of A. Figure 5a plots $A\rho_\infty/\rho_0$ versus water depth for a set of marine sediments (with water depth > 800 m; Table 2, ESM). Data are correlated (99% CL), following $A\rho_\infty/\rho_0$ an exponential decrease with water depth, which explains 96% of its variability. Figure 5b plots A versus water depth for a set of lacustrine environments (from Table 2, ESM). Here the best correlation is obtained through a multiplicative model (99% CL) which explains 89% of the variability in A.

While parameters ρ_∞ and ρ_0 can be estimated from bulk density profiles, the determination of α is subject to large uncertainties, which complicates the estimation of parameters A and C_z. Using only data from Muñoz et al. (2004) in Table 2 (ESM), a mean value of $C = (0.0042 \pm 0.0017)$ year^{-1} was obtained (95% CL, excluding three data with a low quality fit to Eq. 4). For lacustrine environments, variability was larger, with $C_z = (0.050 \pm 0.030)$ year^{-1}.
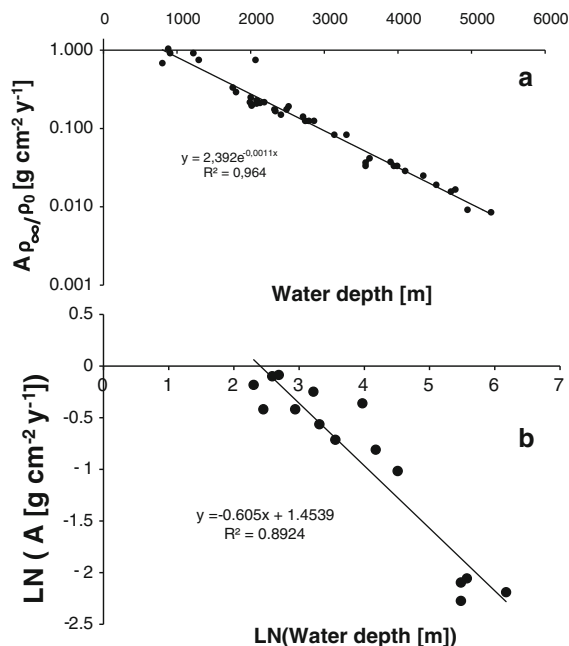
Fig. 6 Sedimentation rates for the Alpine sediment core (Fig. 1 ESM) after the CRS model

Fig. 5 **a** Plot of $A\rho_\infty/\rho_0$ versus water depth for a set of marine sediments. **b** LN(A) versus LN of water depth, for a set of lacustrine sediments. In both cases A was estimated from Eq. 10, using data from Table 2, in the Electronic Supplementary Material

Fig. 7 Bulk density versus depth profile for the Alpine sediment core (data in circles by Erlinger et al. (2008); a relative error of 5% has been assumed). R9 corresponds to model output using best fit to Eq. 4 as initial conditions, a constant $w_0 = 0.1$ g cm^{-2} year^{-1} and $C_z = 0.0560$ year^{-1} (from Eq. 9). Curve R10 is as R9, but with the time-dependent w_0 given by Fig. 6 and $C_z = 0.0392$ year^{-1} (from Eq. 9 and the mean value of w_0)

A test for the hypothesis of acceleration

A situation of particular interest is the occurrence of a plateau or flattening in the unsupported ^{210}Pb versus depth profile in the uppermost sediment layers, which is interpreted by the CRS model (Appleby and Oldfield 1978) as acceleration in recent sedimentation rates. The same profile can be alternatively explained by a zone of complete or incomplete mixing, with a constant sedimentation rate (Robbins and Edgington 1975; Abril et al. 1992). The occurrence of a distinctive ^{137}Cs (or other artificial fallout radionuclide) peak within the ^{210}Pb plateau has been considered as a definitive demonstration of acceleration (Erten et al. 1985), but Abril (2003b, 2004) demonstrated that this fact is not able to provide an unambiguous explanation. As shown in Fig. 4 (curve R7), there is a chance to use the bulk density profile as an additional and independent test for acceleration, if it exists.

Erlinger et al. (2008) measured excess ^{210}Pb specific activity versus depth in a sediment core from an Alpine lake (Fig. 1, ESM). They found a relative flattening in
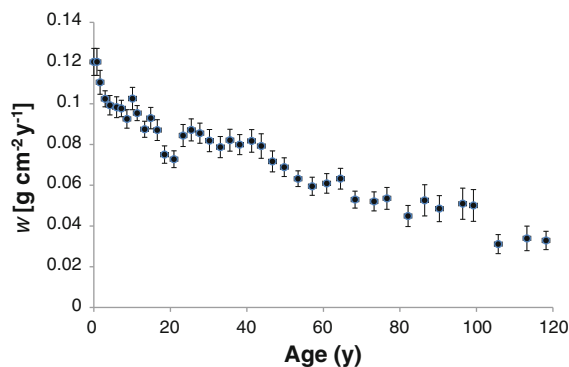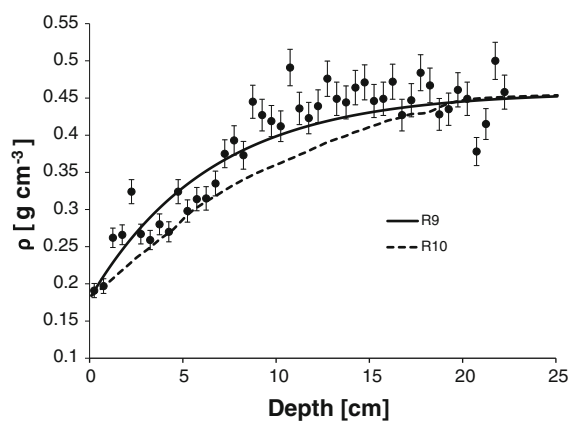
the uppermost layers. The application of the CRS model in the present work provides the sedimentation history given in Fig. 6 (mean value of 0.070 g cm^{-2} year^{-1}), with a clear acceleration trend in recent years. The authors applied the Incomplete Mixing Zone (IMZ) model (by Abril et al. 1992), which reasonably explained the ^{210}Pb profile with a constant sedimentation rate of 0.10 g cm^{-2} year^{-1}. The sediment texture was homogeneous, and grain size ranged from clay to silt. The measured bulk density profile is shown in Fig. 7 (circles). In the absence of reported error measurements, a relative error of 5% has been assumed, a criterion comparable to that one used by Jourabchi et al. (2010).

The best fit ($\chi_v = 1.75$, weighted to one standard error and including the freedom degrees) to Eq. 4 provided $\rho_\infty = 0.458$; $\rho_1 = 0.276$; $\alpha = 0.154$ which will be used as initial conditions in the following modelling exercises.

To test IMZ results, the model used $C_z = 0.0560$ year^{-1} (from Eq. 9) and the same numerical scheme presented in the Methods section. The numerical solution is presented in Fig. 7 (curve R9), which matches the analytical fit (and thus, with $\chi_v = 1.75$). In Fig. 7, the curve R10 shows the corresponding numerical solution using the same initial conditions, $C_z = 0.0392$ year^{-1} (from Eq. 9, and using the averaged value of w_0 from the CRS model in Fig. 6) and the detailed sedimentation history, $w_0(t)$, from Fig. 6 (linear interpolation was used between every two adjacent values). In this case, the numerical solution fails to describe the observed behaviour in bulk densities ($\chi_v = 2.51$). We note that the value of A, estimated from C_z, α and ρ_s, was 0.91 and 0.64 g cm^{-2} year^{-1}, while the one derived from the empirical relationship of Fig. 6 was 0.89, closer to the first case, although it does not properly hold for unsteady-state situations, such as those of varying sedimentation rates.

Discussion

Numerical solutions appropriately reproduced the known analytical ones in the tested exercises.

Moderate periodic oscillations in sedimentation rates hardly could be detected from experimental bulk density profiles with typical uncertainties in measurements (Fig. 4, R4). The situation is substantially different if the amplitude of changes in w_0 was larger (Fig. 4, R4b), in such a way that conduction can exceed the input of material, and then, the SWI collapses (v takes negative values). This produces an irreversible decrease in the scaling factor, which could be confounded by an increase in the sedimentation rate (as in the curve R3 in Fig. 3).

The effects of episodic events of increase/decrease in w_0 were not symmetric, and only the episodic increase produced some noticeable distortion in the bulk density profile. The effect of acceleration in recent sedimentation rates is a noticeable depletion in the bulk density profile, with a distinctive almost linear increase in the uppermost sediment layers.

The modeling exercise of curve R8 (Fig. 4) attempted to simulate changes not in the amount, but in the nature of the incoming material, resulting in different packing properties, and thus in different bulk densities at the SWI, while conductivity remains essentially unchanged. This resulted in noticeable perturbations in the bulk density profile in the uppermost layers of the sediment.

Concerning the behavior of parameter A in marine sediments, we note that $A\rho_\infty/\rho_0$ is proportional to the sedimentation velocity, for which an exponential dependence with water depth in deep sea sediments already has been stated empirically by Middelburg et al. (1997). In terms of sedimentation velocity, the rate of accumulation decreases from near-shore to deep-sea deposits. In terms of conductivity, the slope of the bulk density profile (or the scaling factor) seems to be self-adjusted in order to increase conductivity when sedimentation rates increase (Eq. 9).

The empirical relationships from Fig. 5 can be now used to estimate sedimentation rates from Eq. 10 and compare them against the ones from Table 2 (ESM), but at this point it is a circular argument. Table 2 (ESM) compiles a limited set of data, and a wider survey surely will show a more complex situation, even if limited to properly validated sedimentation rates. But it also illustrates the chance to find suitable correlations. The aim at this stage is just to point out that, after a wider intercomparison, there is a promising possibility to establish suitable empirical formulae for parameter A, and then being able to obtain an estimate of sedimentation rates which could serve, at least, as a first control test in the radiometric dating of recent sediments.

It is worth noting limitations in the test for the hypothesis of acceleration. By using C_z as a free parameter, it is possible to improve the agreement between model and observation, since an increase in C_z produces effects equivalent to a decrease in sedimentation rates. Thus, for a more rigorous use of the present technique, independent constraint for the C_z parameter is needed.

In the particular case shown in Fig. 7, none of the models reproduced the detailed structure of the bulk density profile, which retained a more complex (and interesting) history than the current radiometric dating models could reveal.

Shortening and the mass depth variable

At the present stage we need to improve our level of understanding about the SWI boundary conditions and on the factors affecting conductivity, particularly those that produce irreversibility, or rates of change in conductivities following different trends than the one of Eq. 8. If bulk densities profiles are finally seen as a potential dating tool, it will be then necessary to revisit the technical problems involved in the sediment coring, particularly those related with the shortening of the core (Glew et al. 2001). Meanwhile, it will be advisable to report data on bulk densities in papers concerning the radiometric dating of sediments, to allow the construction of a suitable database for further theoretical and practical developments.

Shortening is perturbation of the actual depth variable, z, with the stratigraphic elements of the core generally being thinned progressively down-core because of the loss of sediment that is pushed laterally outwards ahead of the tube (Glew et al. 2001). Consequently, the mass depth variable also will be affected, but not the bulk density itself because the loss of interstitial water seems to be negligible. Thus, if the length of the core is large enough to include the whole asymptotic increase in bulk density, this shortening will not be a significant problem in the modelling of bulk density profiles.

The storage of the core prior to the sampling in laboratory can produce water losses from the uppermost centimetres. This shortening affects to the bulk volume. It does not affect the measurement of mass depth, but it does affect bulk density near the SWI. This shortening can be methodologically minimized, and if present, the first data for bulk density can be excluded in the fit to estimate its limit values and the scaling factor.

Firstly, equations have to be conveniently rewritten in terms of mass depth variable. From the definition of mass depth, $dm = \rho \, dz$. It is then possible to apply the chain rule for partial derivatives

$$\frac{\partial}{\partial z} = \rho \frac{\partial}{\partial m}.$$

The continuity equation, in terms of the mass depth variable is

$$\frac{\partial \rho}{\partial t} = -\rho \frac{\partial}{\partial m}(\rho v + \beta K), \tag{11}$$

with Eq. 8 transformed into

$$\frac{\partial K}{\partial m} = -C_z \frac{\rho_D}{\rho}. \tag{12}$$

The numerical scheme can be conveniently adapted to the mass depth variable. We note that Eq. 12 does not provide a bulk density profile following Eq. 4. Nevertheless, the following function provides a suitable fit to measured data:

$$\rho(m) = \rho_\infty - \rho_1 e^{-\alpha_m m}. \tag{13}$$

It is worth noting that this fit produces different values for the "equivalent" scaling factor in z-variable. As shown previously, initial conditions do not affect the final steady state, and the relevant problem is the use of an appropriate C_z value. Thus, without need to go into details, the best fit from Eq. 13 will lead to a different scaling factor in the z-space, and then to a different C_z value (from Eq. 9). If Eq. 4 is postulated as the starting point, then it is possible to use a practical potential relationship between z and m to express bulk densities as a function of m, which preserves the use of the scaling factor α and the relationship from Eq. 9.

At this point it is important to note that the use of Eq. 4 is justified only as a practical empirical relationship, but the same could be stated for a function of m. The χ^2 test could be a criterion for selection, but Eq. 12 has additional mathematical advantages when it is used in combination with radiometric dating models (Abril 2003a). Then, if a new law for conductivity is postulated,

$$\frac{\partial K}{\partial m} = -C_m \rho_D, \tag{14}$$

Equation 13 would arise as the steady-state solution. Equation 11 for A, and the empirical relationships from Fig. 5 still hold, and now

$$C_m = A\alpha_m/\rho_s. \tag{15}$$

Figure 2 in ESM shows the bulk density profile for the same sediment core from Fig. 7, but using the mass depth variable. The best fit to Eq. 13 (coincident with curve R11) provided $\alpha_m = 0.558$ cm^{2}g^{-1}, $\rho_\infty = 0.452$; $\rho_1 = 0.267$ g cm^{-3}, with $\chi_v = 1.64$ (vs. $\chi_v = 1.75$ for the best fit to Eq. 4 with z variable—including all the data points in both cases-). The corresponding steady-state C_m value for $w_0 = 0.1$ g cm^{-2} year^{-1} was 0.206 year^{-1}

(0.21 year^{-1} using A from the empirical relationship of Fig. 5b), what leads to curve R11 as the steady-sate solution (after a simulation time of 150 year). Curve R-12 was generated with the time-dependent sedimentation rates from Fig. 6 and $C_m = 0.144$ year^{-1} (from the averaged value of w_0), providing $\chi_v = 2.17$. For the sake of comparison, Fig. 2 (ESM) also includes the best fit (Curve R-13, $\chi_v = 1.39$) obtained excluding the five uppermost data points ($\alpha_m = 0.826$ cm^{2}g^{-1}, $\rho_\infty = 0.447$; $\rho_1 = 0.392$ g cm^{-3}), what points out the important potential effect of the storage-related shortening.

Conclusions

Early compaction produces steep gradients in bulk densities in the uppermost layers of the sediments, which can be described as an exponential-saturation function versus actual depths (z), or versus mass-depth (m). These gradients can be understood in terms of a linear transport equation, which accounts for the mass flow associated with early compaction, and which involves uniform spatial gradients in the compaction potential energy, and depth-dependent conductivities.

When the conductivity shows gradients (vs. z or m) proportional to the "default" bulk density, ρ_D, then the exponential-saturation function (vs. z or m), arises as the steady-state solution.

For typical steady-state bulk density profiles given by Eq. 4 (or 13), the scaling factor is the only relevant parameter to be used for model validation, but it is a function of the ratio C_z/w_0 Consequently w_0 could be obtained by inverse modeling only if C_z (or A) can be independently established.

Empirical relationships can be constructed among the amplitude A, of the conductivity function and water depth, which partly constrains the range of variability of admissible sedimentation rates. Multi-parametric analysis from a suitable data set will be necessary to sufficiently constrict A, and thus to use it for dating purposes. The dependence of A on water depth suggests that sedimentation rates can be coupled to conductivities through the physical construction of the scaling factor.

Transient situations, such those associated with time-dependent sedimentation rates, produce noticeable distortions in bulk density profiles, which can be used to test alternative radiometric dating models. More precisely, at the present stage of theory development, it is possible to recognize from the bulk density profile a transient regimen (as curves R2[$t = 10$ year], R3[$t = 10$ year], R7 and R8 in Figs. 3, 4), but some transient regimens can prove indistinguishable from the steady-state, particularly if some degree of co-variation exists between C_z and w_0.

The mass depth variable can be alternatively used for modeling the bulk density profiles, what shows some advantages in the treatment of storage-related shortening effects.

References

Abril JM (2003a) A new theoretical treatment of compaction and the advective-diffusive processes in sediments. A reviewed basis for radiometric dating models. J Paleolimnol 30:363–370

Abril JM (2003b) Difficulties in interpreting fast mixing in the radiometric dating of sediments using Pb-210 and Cs-137. J Paleolimnol 30:407–414

Abril JM (2004) Constraints on the use of Cs-137 as a time-marker to support CRS and SIT chronologies. Environ Pollut 129:31–37

Abril JM, García-León M (1994) The integrated atmospheric flux effect in a radiogeochronological model. J Environ Radioact 24:65–79

Abril JM, García-León M, García-Tenorio R, Sánchez CI, El-Daoushy F (1992) Dating of marine sediments by an incomplete mixing model. J Environ Radioact 15:135–151

Appleby PG (2001) Chronostratigraphic techniques in recent sediments. In: Last WL, Smol JP (eds) Tracking environmental change using lake sediments. Basin analysis, coring, and chronological techniques. Developments in paleoenvironmental research. Kluwer Academic Publishers, Dordrecht, pp 171–203

Appleby PG, Oldfield F (1978) The concentration of lead-210 dates assuming a constant rate of supply of unsupported ^{210}Pb to the sediment. Catena 5:1–8

Buffoni G, Delfanti R, Papucci C (1992) Accumulation rates and mixing processes in near-surface North Atlantic sediments: evidence from C-14 and Pu-239, 240 down-core profiles. Mar Geol 109:159–170

Chilingarian GV, Rieke HH, Donaldson EC (1995) Compaction of argillaceous sediments. In: Chilingarian GV, Donaldson EC, Yen TF (eds) Subsidence due to fluid withdrawal. Developments in petroleum sciences, vol 41. Elsevier Science B.V., Amsterdam, The Netherlands, pp 47–164

Christensen ER, Bhunia PK (1986) Modeling radiotracers in sediments: comparison with observations in Lakes Huron and Michigan. J Geophys Res 91:8559–8571

Crusius J, Anderson RF (1995a) Sediment focussing in six small lakes inferred from radionuclide profiles. J Paleolimnol 13:143–155

Crusius J, Anderson RF (1995b) Evaluating the mobility of ^{137}Cs, $^{239+240}$Pu and ^{210}Pb from their distributions in laminated lake sediments. J Paleolimnol 13:119–141

Erlinger Ch, Lettner H, Hubmer A, Hofmann W, Steinhäusler F (2008) Determining the Chernobyl impact on sediments of a pre-Alpine lake with a very comprehensive set of data. J Environ Radioact 99:1294–1301

Erten HN, von Gunten HR, Rössler E, Sturm M (1985) Dating of sediments from Lake Zürich (Switzerland) with ^{210}Pb and ^{137}Cs. Schwiz Z Hydrol 47:5–11

Fukumori E, Christensen ER, Klein RJ (1992) A model of ^{137}Cs and other tracers in lake sediments considering particle size and the inverse solution. Earth Planet Sci Lett 114:85–99

Glew JR, Smol JP, Last WM (2001) Sediment core collection and extrusion. In: Last WL, Smol JP (eds) Tracking environmental change using lake sediments. Basin analysis, coring, and chronological techniques. Developments in paleoenvironmental research. Kluwer Academic Publishers, Dordrecht, pp 171–203

Jourabchi P, L'Heureux I, Meile Ch, Van Cappellen Ph (2010) Physical and chemical steady-state compaction in deep-sea sediments: role of mineral reactions. Geochim Cosmochim Acta 74:3494–3513

Laissaoui A, Benmansour M, Ziad N, Ibn Majah M, Abril JM, Mulsow S (2008) Anthropogenic radionuclides in the water column and a sediment core from the Alboran Sea: application to radiometric dating and reconstruction of historical water column radionuclide concentrations. J Paleolimnol 40:823–833

Meysman FJR, Boudreau BP, Middelburg JJ (2005) Modeling reactive transport in sediments subject to bioturbation and compaction. Geochim Cosmochim Acta 69:3601–3617

Middelburg JJ, Soetaert K, Herman PMJ (1997) Empirical relationships for use in global diagenetic models. Deep Sea Res 44:327–344

Muñoz P, Langeb CB, Gutiérrez D, Hebbeln D, Salamanca MA, Dezileau L, Reyss JL, Benninger LK (2004) Recent sedimentation and mass accumulation rates based on ^{210}Pb along the Peru–Chile continental margin. Deep Sea Res 51:2523–2541

Robbins JA (1978) Geochemical and geophysical applications of radioactive lead isotopes. In: Nriago JP (ed) Biochemistry of lead in the environment. Elsevier, Amsterdam, pp 285–393

Robbins JA, Edgington DN (1975) Determination of recent sedimentation rates in Lake Michigan using ^{210}Pb and ^{137}Cs. Geochim Cosmochim Acta 39:285–304

Robbins JA, Holmes C, Halley R, Bothner M, Shinn E, Graney J, Keeler G, tenBrink M, Orlandini KA, Rudnick D (2000) Time-averaged fluxes of lead and fallout radionuclides to sediments in Florida Bay. J Geophys Res 105:28805–28821

Smith JN (2001) Why should we believe ^{210}Pb sediment geochronologies? J Environ Radioact 55:121–123

Wan GJ, Santschi PH, Sturm M, Farrenkothen K, Lueck A, Werth E, Schuler Ch (1987) Natural (210Pb, 7Be) and fallout (137Cs, 239, 240Pu, 90Sr) radionuclides as geochemical tracers of sedimentation in Greifensee, Switzerland. Chem Geol 63:181–196